Strain Engineering a Multiferroic Monodomain in Thin-Film $BiFeO_3$

N. Waterfield Price,[1,*] A.M. Vibhakar,[1] R.D. Johnson,[1,2] J. Schad,[3] W. Saenrang,[3,†] A. Bombardi,[4] F.P. Chmiel,[1] C.B. Eom,[3] and P.G. Radaelli[1]

[1] *Clarendon Laboratory, Department of Physics, University of Oxford, Parks Road, Oxford OX1 3PU, United Kingdom*

[2] *ISIS Facility, Rutherford Appleton Laboratory, Chilton, Didcot OX11 0QX, United Kingdom*

[3] *Department of Materials Science and Engineering, University of Wisconsin-Madison, Madison, Wisconsin 53706, USA*

[4] *Diamond Light Source Ltd., Harwell Science and Innovation Campus, Didcot OX11 0DE, United Kingdom*

(Received 31 August 2018; revised manuscript received 7 January 2019; published 13 February 2019)

The presence of domains in ferroic materials can negatively affect their macroscopic properties and hence their usefulness in device applications. From an experimental perspective, the measurement of materials comprising multiple domains can complicate the interpretation of the material properties and their underlying mechanisms. In general, $BiFeO_3$ films tend to grow with multiple magnetic domains and often contain multiple ferroelectric- and ferroelastic-domain variants. By growing (111)-oriented $BiFeO_3$ films on an orthorhombic $TbScO_3$ substrate, we are able to overcome this and, by exploiting the magnetoelastic coupling between the magnetic and crystal structures, bias the growth of a given magnetic-, ferroelectric-, and structural-domain film. We further demonstrate the coupling of the magnetic structure to the ferroelectric polarization by showing that the magnetic polarity in this domain is inverted upon 180° ferroelectric switching.

DOI: 10.1103/PhysRevApplied.11.024035

I. INTRODUCTION

The coupling of spontaneous electric, magnetic, and elastic orders within single-phase materials, known as multiferroics, could provide a platform for a new generation of memory devices combining nonvolatile storage with efficient switching mechanisms [1–3]. This unique technological promise can only be fulfilled by achieving an exquisite control over *multiferroic domains* [4], which form as a direct consequence of spontaneous symmetry breaking. Furthermore, from an experimental perspective, the intrinsic properties of a prototypical device can be obscured by the presence of multiple domains and would ideally be demonstrated within a single-domain architecture. Although the exploitation of particular combinations of domains can be advantageous [5–8], their population and the exact location of the domain boundaries must be controlled with great precision to realize the full potential of multiferroic materials.

A classic illustration of this challenge is provided by $BiFeO_3$ (BFO), one of the most studied multiferroics [9]. At room temperature, BFO is at the same time ferroelectric (FE), ferroelastic, and antiferromagnetic (cycloidal) [10,11]. Below the ferroelectric phase transition $T_C \sim 1100$ K, BFO has a polar $R3c$ perovskite structure with a rhombohedral distortion along the (pseudocubic) $[111]_{pc}$ direction [12]. This allows for four possible ferroelastic domains, (labeled $r_{1–4}$ according to the notation of Streiffer *et al.* [13]), each corresponding to the distortion being along each of the $\langle 111\rangle_{pc}$ pseudocubic body diagonals, as shown in Fig. 1(a). Within each of these ferroelastic domains, there are two possible ferroelectric domains, r_i^+ and r_i^-, with the polarization $\mathbf{P}$ along the $\pm[111]_{pc}$ directions [14]. Magnetic ordering occurs below $T_N \sim 640$ K, where the Fe spins order with a long-period cycloidal magnetic structure. This breaks the threefold rotational symmetry and, for each ferroelectric domain, results in three symmetry-equivalent $\mathbf{k}$ domains, with magnetic propagation vectors $\mathbf{k}_1 = (\delta, \delta, 0)_h$, $\mathbf{k}_2 = (\delta, -2\delta, 0)_h$, and $\mathbf{k}_3 = (-2\delta, \delta, 0)_h$, where the subscript h denotes the hexagonal setting and $\delta \sim 0.0045$ at room temperature [11,15]. In fact, it has recently been reported that the structure of both bulk [16] and thin-film [17,18] BFO is monoclinic with broken threefold symmetry. In this case, these monoclinic domains are coupled one-to-one to the magnetic $\mathbf{k}$ domains, resulting in three possible *magnetostructural* domains. Each of these magnetostructural domains can support two possible directions of the magnetic polarity $\boldsymbol{\lambda}$, which is defined as $\boldsymbol{\lambda} = \mathbf{k} \times (\mathbf{S}_i \times$

*noah.waterfieldprice@physics.ox.ac.uk

†Present address: School of Physics, Institute of Science, Suranaree University of Technology, Nakhon Ratchasima, 30000, Thailand

$\mathbf{S}_j$), where $\mathbf{S}_i$ and $\mathbf{S}_j$ are spins on adjacent sites along the direction of $\mathbf{k}$, and can be thought of as characterizing the "sense of rotation" of the cycloidal structure (for more detail, see Supplemental Material S-IV [19]). It is understood that the magnetic polarity is directly coupled to the ferroelectric polarization via the direct Dzyaloshinskii-Moriya interaction [20], giving combined ferroelectric-magnetopolar domains. In summary, there are

$$\overbrace{N_{\text{ferroelastic}}}^{4} \times \overbrace{N_{\text{ferroelectric-magnetopolar}}}^{2} \times \overbrace{N_{\text{magnetostructural}}}^{3} = 24$$

possible domain variants.

In epitaxial films, the relative proportion of these domains can be manipulated. For instance, the ferroelastic-domain populations of BFO may be tailored through certain choices of film orientation, substrate symmetry, and miscut [21]. BFO films grown in the $(001)_{pc}$ orientation on cubic $SrTiO_3$ (STO) substrates typically display all four ferroelastic domains. The number of ferroelastic variants can be reduced to two by growing BFO on a lower-symmetry substrate, for example, orthorhombic $(001)_{pc}$-$TbScO_3$ (TSO) [22]. Alternatively, the use of a $(001)_{pc}$-STO substrate miscut by 4° toward the $[100]_{pc}$ direction favors the two ferroelastic domains with their rhombohedral distortion along the miscut direction [23] and, similarly, a miscut toward $[110]_{pc}$ instead results in a single ferroelastic domain [21]. A ferroelastic monodomain may also be achieved by growing a $(111)_{pc}$-oriented film on an STO substrate, resulting in a single ferroelastic domain, with its rhombohedral distortion aligned with the $(111)_{pc}$ surface-normal direction [18]. The ferroelectric-domain population can be controlled by applying an electric field or by including a metallic $SrRuO_3$ buffer layer between the substrate and the BFO film, which screens the depoling field of the BFO and results in the electrical polarization favoring directions with a downward component (into the film) [24]. Although it is relatively straightforward to control the ferroelectric domain populations at growth, BFO-based ferroelectric devices are plagued by polarization fatigue and electrical-breakdown problems [25]. This has been attributed to a nondeterministic multistage switching process that causes the film to break up into multiple ferroelastic domains, resulting in charged domain walls and domain pinning [26]. Even though they can be grown as a ferroelectric monodomain, this issue is most pronounced in the $(111)_{pc}$-oriented films, as this orientation preserves the intrinsic threefold symmetry of the crystal structure, making all possible switching pathways equally likely.

By contrast, antiferromagnetic domains are more difficult to manipulate because, unlike ferromagnets and ferroelastics, antiferromagnets do not couple to a uniform conjugated field (a field that couples to the order parameter to yield a contribution to the total energy). Yet achieving this control is crucial, because most device configurations

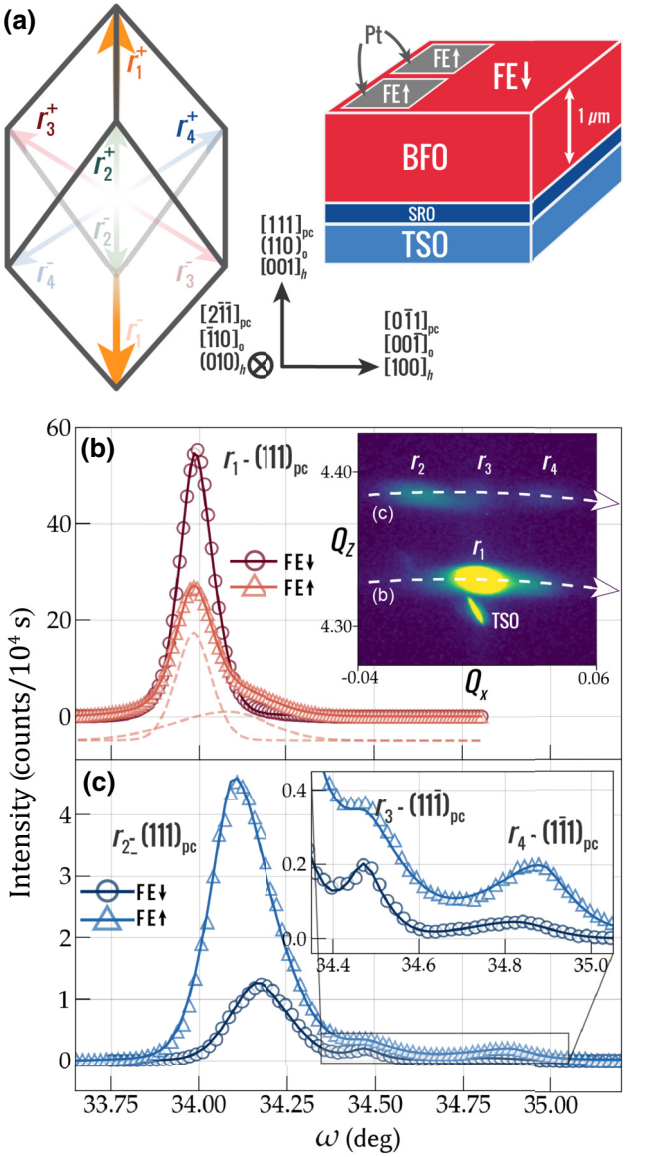

FIG. 1. The effect of switching on ferroelastic domains of BFO/TSO. (a) A schematic depiction of the unique $[111]_{pc}$ axes in each of the four ferroelastic domains, shown in the pseudocubic unit cell viewed along the $\mathbf{b}_h^*$ direction. The $[111]_{pc}$ axes are labeled $r_{1–4}$, with the "+/−" superscript denoting the corresponding ferroelectric domain (see the text). The crystallographic relationship between the hexagonal and pseudocubic BFO unit cells and the orthorhombic TSO unit cell is indicated by the black axes. Rocking-curve scans of the (b) $(111)_{pc}$ reflection of the majority r_1 ferroelastic domain and (c) $(\bar{1}11)_{pc}$, $(11\bar{1})_{pc}$, and $(1\bar{1}1)_{pc}$ reflections corresponding to each of the minority r_2, r_3, and r_4 domains, respectively. Data for the as-grown FE ↓ and switched FE ↑ states are shown by the dark circles and light triangles, respectively. Fits to the data are shown by the solid lines and the dotted light red lines in (b) show the two peak profiles contributing to the intensity in the FE ↑ state. The reciprocal space map shown in the inset is based on laboratory data (for more details, see Supplemental Material S-I [19]), on which we indicate the position of the scans in (b) and (c).

include a ferromagnetic overlayer that is exchange coupled to antiferromagnetic spins. Although some control of propagation vectors using electric fields [27] and high magnetic fields [28] has been demonstrated, a robust method to bias a single propagation vector has yet to be found. Previously, single-magnetic-domain BFO had only been achieved in ultrathin $(001)_{pc}$-oriented films grown on a $NdGaO_3$ substrate [29], where films above a threshold thickness of approximately 5 nm were found to revert to a multidomain state. The recent discovery of a very strong magnetoelastic coupling [17] in BFO affords a potentially new "handle" on magnetic domains. For example, we have previously shown that $(001)_{pc}$-BFO films on miscut STO consist of a single antiferromagnetic domain [30], because the propagation vector oriented in the plane of the film is favored over the other two. By contrast, for $(111)_{pc}$-oriented BFO films grown on STO, the high symmetry of the substrate makes magnetic-domain control extremely challenging. Typical $(111)_{pc}$-oriented BFO films consist of a mosaic of magnetoelastic domains at the submicron scale, in which the three magnetic domains are equally represented [17].

In this paper, we demonstrate the ability to bias the growth of a given structural, ferroelastic, ferroelectric, and magnetic domain in a 1 μm-thick $(111)_{pc}$-oriented BFO film by breaking the threefold symmetry with an orthorhombic TSO substrate. Remarkably, the substrate is able to bias the growth of a majority magnetostructural domain, in spite of the fact that most of the film is relaxed away from the substrate lattice parameters. After multiple switches of the ferroelectric polarization, the majority of the sample (about 80%) remains in the same ferroelastic and magnetoelastic state, while about 19% of the sample converts to a specific alternate ferroelastic domain as a result of a more deterministic switching mechanism. Nonresonant x-ray magnetic scattering (NXMS) with polarization analysis was employed to determine the magnetic polarity of the film and to observe its inversion after ferroelectric switching.

II. EXPERIMENTAL DETAILS

Epitaxial 1-μm-thick films of $(111)_{pc}$-oriented BFO films are grown using double-gun off-axis sputtering [31] onto a TSO substrate oriented with the $(110)_o$ direction specular (the subscript "o" indicates the *Pnma* orthorhombic setting). This direction approximates the $(111)_{pc}$ direction of a simple perovskite, but has an in-plane anisotropy due to the orthorhombicity. The BFO layer grows such that the $\mathbf{a}_h$ axis is antiparallel to the $\mathbf{c}_o$ axis of the TSO substrate. Before depositing the BFO layer, a 30-nm-thick $SrRuO_3$ (SRO) layer is deposited on the TSO substrate by 90° off-axis sputtering. The role of this layer is twofold: first, it elastically biases the film to grow as a ferroelectric monodomain [24] and, second, it acts as a bottom electrode. After the BFO has been grown, 500 μm $\times$ 200 μm $\times$ 10 nm Pt top electrodes are patterned on the film surface using photolithography. This setup allows switching of the ferroelectric polarization under the electrodes along the $(111)_{pc}$ direction (out of plane). BFO films that are 1 μm thick and $(111)_{pc}$ oriented are similarly grown on $(111)_{pc}$-oriented STO substrates, details of which can be found in Ref. [17]. The films grown both on TSO and STO substrates show excellent ferroelectric characteristics (see Supplemental Material S-III [19]), with remnant polarizations of 108 μC cm^{-1} and 110 μC cm^{-1}, respectively, comparable to the highest values reported for BFO films [32].

The synchrotron x-ray measurements, including both the structural characterization and nonresonant-x-ray-magnetic-scattering (NXMS) measurements, are performed on beam line I16, Diamond Light Source (United Kingdom), using a six-circle kappa diffractometer in reflection geometry. Additional measurements are performed on a Rigaku SmartLab four-circle laboratory-based x-ray diffractometer fitted with a Cu K_α x-ray source (see Supplemental Material S-I [19]). For both structural characterization and the NXMS measurements, the incident synchrotron x-ray beam energy is tuned to 4.9 keV, which is off resonance of all chemical elements present in the sample. This energy is high enough that air scattering is minimal, while the NXMS signal can still be relatively easily separated from multiple scattering processes. Conversion of the incident x-ray polarization from linear to circular is achieved using a 100-μm-thick diamond quarter-wave plate. For the NXMS measurements, the scattered x-ray polarization is determined using a pyrolytic-graphite polarization-analyzer crystal, scattering at the (004) reflection. The x-ray beam size at the sample is adjusted by means of slits from approximately 300 μm $\times$ 50 μm to approximately 50 μm $\times$ 50 μm to allow a variable area of the sample, including a small spot under the electrodes, to be illuminated. For all the NXMS measurements, we use an avalanche photodiode detector, positioned after the polarization-analyzer crystal, while the structural characterization measurements are performed using a Pilatus photon-counting area detector. Single-crystal neutron-diffraction measurements are performed on the WISH instrument at ISIS, the United Kingdom pulsed Neutron and Muon Spallation Source. The neutron beam size at the sample position is approximately 20 mm $\times$ 40 mm, thus illuminating the entire film. All the NXMS and neutron-diffraction measurements are taken at room temperature.

III. RESULTS AND DISCUSSION

A. Structural and magnetic characterization of the unswitched sample

The ferroelastic domain population of the unswitched sample (FE ↓) is determined from reciprocal space scans

measured on beam line I16, in which two-dimensional (2D) images from the Pilatus detector are collected as a function of the rocking angle ω. Intensities integrated along particular lines in reciprocal space (corresponding to rocking curves) are shown in Figs. 1(b) and 1(c), while corresponding 2D laboratory data are reported in Supplemental Material S-I [19]. The four possible ferroelastic domains are labeled $r_{1\text{–}4}$, as shown in Fig. 1(a). The r_1 domain has its rhombohedral axis aligned perpendicular to the film, so that the $(111)_{\text{pc}}$ reflection is surface normal. The $(\bar{1}11)_{\text{pc}}$, $(\bar{1}\bar{1}1)_{\text{pc}}$, and $(11\bar{1})_{\text{pc}}$ reflections of the $r_{2\text{–}4}$ domains are nearby in reciprocal space but have a slightly shorter d-spacing and form a triangle around the $(hhh)_{\text{pc}}$ axis of the r_1 domain, indicative of coherent twinning. Note that, by the geometry of the measurement, this triangle is projected into a single arc in the reciprocal space map shown in the inset of Figure 1(b). Almost 96% of the sample is found to be in the r_1 domain, which has a narrow rocking curve [Fig. 1(b)] with $\Delta\omega_{\text{FWHM}} \sim 0.1^\circ$. The r_2 population is approximately 3.7%, which is significantly greater than for films grown on STO. The rocking curves of the minority domains $r_{2\text{–}4}$ [Fig. 1(c)] are somewhat broader ($\Delta\omega_{\text{FWHM}} \sim 0.2^\circ$) than for r_1.

Next, we probe the magnetic structure of the majority (r_1) ferroelastic domain by NXMS and neutron diffraction. We measure the magnetic satellite reflections corresponding to the long-range incommensurate magnetic ordering, which occur near the $\mathbf{N} = (0, 0, 3(2n+1))_h$ reciprocal lattice positions at which (Thomson) charge scattering is forbidden due to the c glide.

The diffraction pattern expected from each of the magnetic $\mathbf{k}$ domains is a pair of peaks at positions $\mathbf{N} \pm \mathbf{k}_i$, where $\mathbf{k}_i$ is the propagation vector of the corresponding magnetic domain. Hence, if the populations of all three magnetic domains are illuminated, one should observe a star of six satellite peaks. For $(111)_{\text{pc}}$-oriented BFO films grown on STO, we have previously shown that these six peaks merge in pairs to form a triangle of peaks, due to the presence of magnetostructural domains on a submicron scale [17] [NXMS and neutron-diffraction data from STO-grown samples are reproduced in Figs. 2(a) and 2(c)]. Figure 2(b) shows a reciprocal space map of the TSO-grown sample measured by NXMS about the $\mathbf{N} = (009)_h$ reciprocal lattice position measured in a region of the film in its as-grown "virgin" state. These data are collected using linearly polarized incident light with $\mathbf{E}$ normal to the scattering plane while only detecting scattered light with $\mathbf{E}$ in the scattering plane (a polarization-analyzer angle of $\eta = 90^\circ$). In sharp contrast with the BFO/STO data, we observe only a *single pair of satellite peaks* at positions $\mathbf{N} \pm \mathbf{k}_2$. Therefore, in the region of the film illuminated by the x-ray spot, the r_1 ferroelastic domains support a single magnetic domain. We repeat this measurement at several sample locations over two identically grown BFO/TSO films and obtain identical results at all positions. To further test this magnetoelastic coupling, we measure an equivalent unswitched film using neutron diffraction and the corresponding reciprocal space map about the $(003)_h$ position is shown in Fig. 2(d). Given that the neutron beam illuminates the entire sample, this verifies that all of the r_1 domains comprise a magnetic monodomain. The fitting of a theoretical intensity calculation to both the x-ray and neutron data simultaneously yields a propagation vector of $\delta = 0.0042(1)$ Å^{-1}. The propagation vector of the cycloidal domain is $\mathbf{k}_2$, which is aligned along the $[001]_o$ direction of the TSO substrate. We also note the absence of any diffuse tails of intensity extending between the two satellite peaks and the $(009)_h$ position, as is seen in $(111)_{\text{pc}}$-oriented BFO films grown on STO substrates [17]. This indicates that the magnetic structure is largely coherent throughout the film and is consistent with the hypothesis that the small domain size in the multidomain BFO/STO films is an important factor in the disorder resulting in the diffuse scattering observed in those films. Given that these films are grown as FE monodomains, one expects that the magnetic structure constitutes a monodomain not only in terms of having a single propagation vector but also a single magnetic polarity. The magnetic polarity is further explored in Sec. III C. Although time-inversion and/or phase-slip domains may still be present, these would not affect the ability of the BFO film to exchange couple to a ferromagnetic overlayer.

B. Structural and magnetic characterization of the switched sample

Additional structural and magnetic diffraction data are collected from a spot directly underneath an electrode. This part of the BFO film is electrically switched by a single half-cycle of the ferroelectric hysteresis loop (FE ↑) (see Fig. 5 within the Supplemental Material [19]). The rocking curves of the four ferroelastic domains are reported in Figs. 1(b) and 1(c), with the same conventions as for the unswitched sample. There are two main effects to be noted: first, part of the intensity is transferred from the r_1 to the r_2 domain and, second, the $(111)_{\text{pc}}$ reflection of the r_1 domain broadens. After switching, the r_1 intensity is well modeled with a sharp peak (which we continue to label r_1) centered at the same position and with a similar width to the unswitched peak but approximately half the intensity, plus a broader peak, which we will refer to as r_1', shifted by approximately 0.1° to higher ω. The presence of this broad peak indicates that the switching process results in a significant population of incoherent ferroelastic domains, the c axes of which are slightly misaligned with respect to the sample surface normal direction. Both the bulk ferroelectric measurements (see Supplemental Material S-I [19]) and the NMXS polarimetry data (see Sec. III C) indicate that the electric polarization has been switched in most of the sample under the electrode.

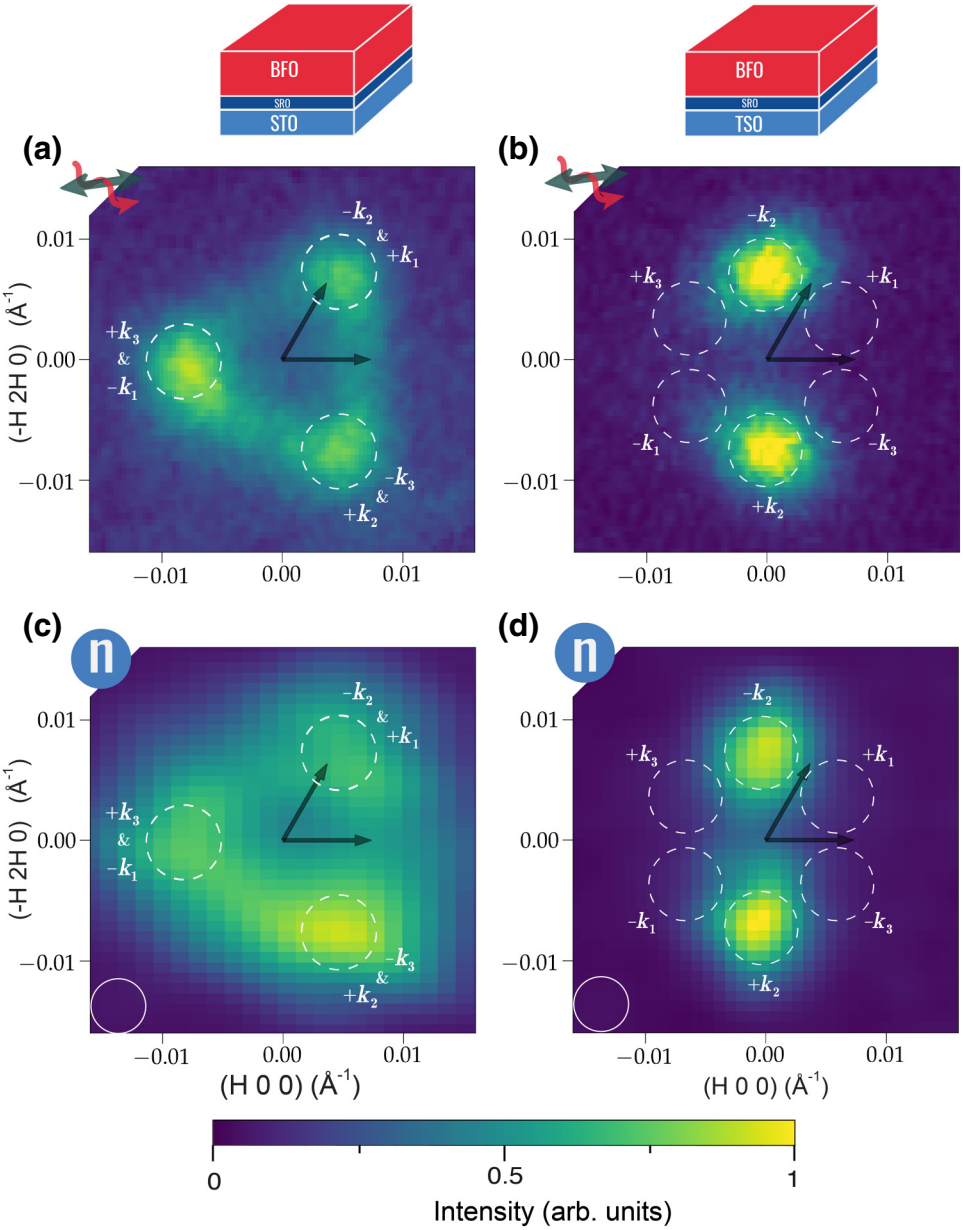

FIG. 2. Magnetic x-ray and neutron-diffraction reciprocal space maps of BFO/STO and BFO/TSO. Reciprocal space maps about the $(009)_h$ position measured by NXMS with linearly polarized incident x rays for (a) BFO/STO and (b) BFO/TSO. Reciprocal space maps about the $(003)_h$ position measured by neutron diffraction for (c) BFO/STO and (d) BFO/TSO. The BFO/STO neutron data in (c) are reproduced from Ref. [17] and the x-ray data in (a) are measured on the same sample using the method described in Ref. [17]. The expected positions of the magnetic satellite peaks for the two different substrates are indicated by the dashed circles. The white circle in the lower-left corner of (c) and (d) indicates the instrumental resolution of the neutron measurements (the x-ray resolution is smaller than the pixel size). Due to the lower sensitivity of the single-crystal neutron measurements to the lattice parameters, the neutron data are scaled to the lattice parameters determined from the higher-resolution x-ray measurements. The reciprocal lattice directions (in the hexagonal setting) are indicated by the translucent black arrows. All measurements are taken at room temperature.

The relative ferroelastic domain populations for the unswitched and switched states are listed in Table I and we see that over half the population of the r_1 domain has been lost, most of which has moved into r_1' and r_2, and that domain populations of r_3 and r_4 have increased only slightly. The skewed populations of the $r_{2\text{–}4}$ domains after switching has important implications for the FE-switching mechanism. It has been demonstrated that 180° switching in $(111)_{pc}$-BFO films occurs via a stochastic multistep switching path consisting of three 71° switching events via the intermediate FE-ferroelastic states [25]. In the said study, Baek *et al.* report that, after many switching cycles

TABLE I. The ferroelastic domain fractions for the as-grown FE ↓ and switched FE ↑ states, obtained from least-squares regression to the data shown in Figure 1.

	Domain populations (%)				
State	r_1	r_1'	r_2	r_3	r_4
FE ↓	95.77(2)	···	3.77(7)	0.31(2)	0.14(1)
FE ↑	46.73(41)	33.61(100)	18.12(16)	0.77(5)	0.76(4)

of $(111)_{pc}$-BFO/STO, they observe equal populations of the three intermediate ferroelastic domains. This is consistent with the fact that three nonsurface-normal BFO ferroelastic domains are symmetry equivalent by the threefold axis of the $(111)_{pc}$-STO substrate. In the present case, the TSO substrate has imposed a *preferential switching pathway* through the r_2 domain. This also follows naturally from symmetry considerations, as the orientation of the $r_{2\text{–}4}$ domains with respect to the orthorhombic $\mathbf{c}_o$ axis breaks the symmetry between r_2 (tilted perpendicularly to $\mathbf{c}_o$) and r_3/r_4 (tilted along directions containing equal and opposite components parallel to $\mathbf{c}_o$).

The magnetic reflections of the switched state are found to be significantly broader (see Supplemental Material S-III [19]), consistent with the reduced crystalline quality of the film upon switching, i.e., size effects from smaller ferroelastic domains and the introduction of structural disorder.

C. NMXS polarimetry

To further probe the magnetic structure of the BFO/TSO monodomain film, we measure the polarization dependence of the magnetic scattering. Here, our approach is very similar to that employed for the STO sample [17]. Using linear horizontal, left-, and right-circular-polarized incident x rays, we measure reciprocal space scans through both $\mathbf{N} \pm \mathbf{k}_2$ magnetic satellite peaks as a function of the polarization-analyzer angle. These measurements are highly sensitive to both the plane of rotation and the magnetic polarity of the cycloidal magnetic structure [17,33]. A model parametrized in terms of the cycloid plane, the

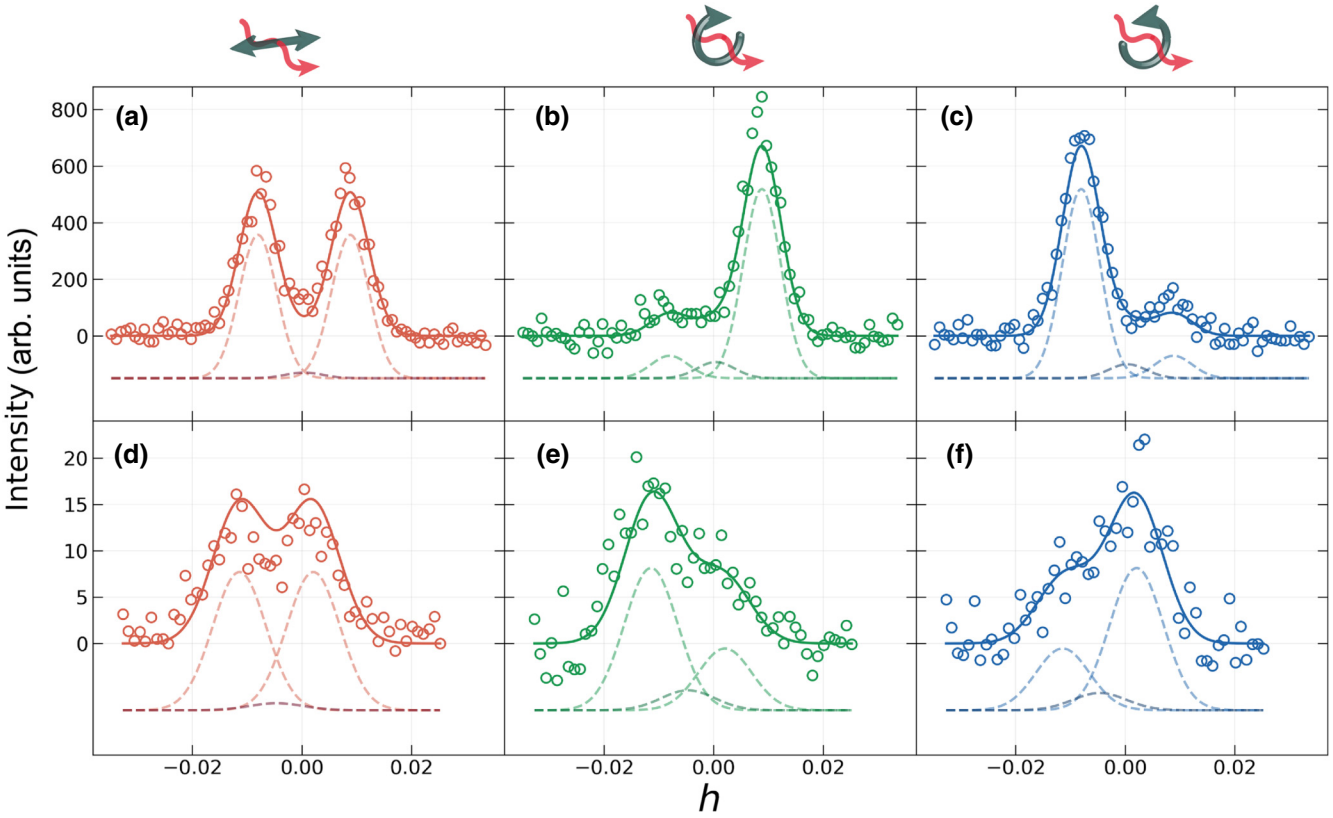

FIG. 3. The polarization dependence of the NXMS intensity of the $\pm\mathbf{k}_2$ satellite peaks. Reciprocal space scans through the $(009)_h \pm \mathbf{k}_2$ peaks of a BFO/TSO film of the unswitched (a)–(c) and switched (d)–(f) states, measured with incident linear horizontal (left), circular left (middle), and circular right (right) polarized x rays, as indicated by the arrows above the axes. The circles show the experimentally measured intensities and the solid lines show the results of a least-squares refinement of the scattered intensity for a single cycloidal domain. The dashed lines show the individual peak contributions of the refined model, comprising the two magnetic satellite peaks and a small multiple scattering peak centered between them (see Supplemental Material S-II [19]). These have been offset for clarity. All measurements are taken at room temperature.

propagation vector, the magnetic polarity, a small multiple scattering peak at the $(009)_h$ position, the peak parameters, a (polarization-dependent) constant background, and a depolarization factor is fitted to the data (for more details, see Supplemental Material S-II [19]).

Figures 3(a)–3(c) show selected reciprocal space scans measured with a polarization-analyzer angle of $\eta = 90^\circ$, with the result of the above least-squares refinement shown as solid lines. The theoretical intensity ratio of the two diffraction peaks, for incident circularly polarized x rays and at this polarization-analyzer angle, is given by (see Supplemental Material S-II [19])

$$\frac{I_{+\mathbf{k}_2}}{I_{-\mathbf{k}_2}} \approx \frac{1+\beta\gamma}{1-\beta\gamma}, \tag{1}$$

where $\gamma = +1$ or -1 for left-circular and right-circular polarized light, respectively. The sign of the magnetic polarity is parametrized by $\beta = -[(\boldsymbol{\lambda}\cdot\hat{\mathbf{n}})/|\boldsymbol{\lambda}|]$, where $\hat{\mathbf{n}}$ is the film surface normal. In agreement with previous studies both on bulk single crystals [20] and films (grown on STO substrates) [34], we find experimentally that $\beta = -1$ for the FE $\downarrow$ state, such that the magnetic polarity is aligned antiparallel to the FE polarization.

The model fits the data extremely well, with a reduced chi-squared statistic of $\chi_\nu = 1.24$, and we thus find that the data is most consistent with a cycloidal magnetic structure with spins rotating in a plane containing the $[001]_h$ (out-of-plane) direction and the $\mathbf{k}_2$ (in-plane) propagation-vector direction, i.e., the same magnetic structure as for the bulk [11,20]. These scans further corroborate that the r_1 domain is a monodomain in the magnetic polarity, as the opposite magnetic polarity would have the opposite circular-polarization dependence.

To test the response of the magnetic structure to 180° electrical switching within the majority r_1/r_1' domain [35], we measure the NXMS signal from regions of the film that have been switched into the FE $\uparrow$ state. Figures 3(d)–3(f) show, for a region of the film switched into the FE $\uparrow$ state, reciprocal space scans through the $\mathbf{N} \pm \mathbf{k}_2$ magnetic satellite peaks measured with incident linear horizontal circular-left- and circular-right-polarized x rays, respectively. It is clear that the polarization dependence of the scattered intensity for left- and right-circular-polarized x rays is inverted between the two FE-polarization states and, as expected, the linear polarization dependence remains the same. A simultaneous fit of the polarization-analyzer scans, including both the switched and unswitched data, demonstrates a 79(4)% switch of the magnetic polarity from the as-grown FE $\downarrow$ state to the switched FE $\uparrow$ state. When performing an equivalent measurement on a multi-**k**-domain $(111)_{pc}$-BFO/STO film, we observe a 93(1)% switch of the magnetic polarity upon inverting the ferroelectric polarization [34]. In both cases, it is possible that the unswitched fraction is due to pinned FE $\downarrow$ domains at the SRO/BFO interface, or that some of the film relaxed back in to the FE $\downarrow$ state, and the magnitude of these effects is enhanced by the TSO substrate.

IV. CONCLUSION

In summary, by using anisotropic epitaxial strain from an orthorhombic TSO substrate in the growth of $(111)_{pc}$-oriented BFO films, we find that we are able to bias the growth of a majority ferroelastic domain. We then demonstrate that this ferroelastic domain supports a single magnetic cycloidal **k** domain. Using x-ray polarimetry, we are able to confirm that this magnetic domain is also of a single cycloidal magnetic polarity. As for previous multidomain devices grown on STO substrates [34], we are able to locally address a prototypical device structure and we find that the magnetic polarity is inverted upon reversal of the FE polarization. Finally, we find that, by using the orthorhombic TSO substrate, we are able to bias a preferential FE-switching pathway.

The strain control of the magnetic state and FE-switching pathways of thin-film BFO demonstrated in this work are both critical ingredients if one is to achieve deterministic and robust operation of a BFO-based device. However, the presence of a finite population of minority ferroelastic domains presents a potential hurdle in realizing such a device. Future investigations could focus on tuning the anisotropic epitaxial strain to eliminate the minority-domain populations, which could potentially stabilize the switching process, eliminating the effects of polarization fatigue.

In accordance with the EPSRC policy framework on research data, access to the data is available at the link given in Ref. [36].

ACKNOWLEDGMENTS

We would like to thank Pascal Manuel for assistance with the neutron-diffraction measurements. We acknowledge Diamond Light Source for time on beam line I16 under Proposals MT15087-1 and MT17291-1. The work done at the University of Oxford (N.W.P., A.M.V., R.D.J., F.P.C., and P.G.R.) was funded by EPSRC Grant No. EP/M020517/1, entitled the Oxford Quantum Materials Platform Grant. The work at the University of Wisconsin-Madison (W.S., J.S., and C.B.E) was supported by the Army Research Office through Grant No. W911NF-13-1-0486. R.D.J. acknowledges support from a Royal Society University Research Fellowship.

[1] S-W. Cheong and M. Mostovoy, Multiferroics: A magnetic twist for ferroelectricity, Nat. Mater. **6,** 13 (2007).

[2] D. Khomskii, Trend: Classifying multiferroics: Mechanisms and effects, Physics **2**, 20 (2009).
[3] M. Fiebig, T. Lottermoser, D. Meier, and M. Trassin, The evolution of multiferroics, Nat. Rev. Mater. **1**, 16046 (2016).
[4] A ferroic domain is a contiguous region of a crystal over which the ferroic order parameter maintains a constant value (and orientation for nonscalar order parameters). A multiferroic domain is where this condition is satisfied for multiple order parameters; for example, in $BiFeO_3$ these order parameters are the polarization, strain, and magnetic polarity.
[5] L. W. Martin, Y-H. Chu, M. B. Holcomb, M. Huijben, P. Yu, S.-J. Han, D. Lee, S. X. Wang, and R. Ramesh, Nanoscale control of exchange bias with $BiFeO_3$ thin films, Nano Lett. **8**, 2050 (2008).
[6] J. Seidel, Lane W. Martin, Q. He, Q. Zhan, Y. H. Chu, A. Rother, M. E. Hawkridge, P. Maksymovych, P. Yu, M. Gajek, N. Balke, S. V. Kalinin, S. Gemming, F. Wang, G. Catalan, J. F. Scott, N. A. Spaldin, J. Orenstein, and R. Ramesh, Conduction at domain walls in oxide multiferroics, Nat. Mater. **8**, 229 (2009).
[7] J. T. Heron, M. Trassin, K. Ashraf, M. Gajek, Q. He, S. Y. Yang, D. E. Nikonov, Y. H. Chu, S. Salahuddin, and R. Ramesh, Electric-Field-Induced Magnetization Reversal in a Ferromagnet-Multiferroic Heterostructure, Phys. Rev. Lett. **107**, 217202 (2011).
[8] Z. Gu *et al.*, Resonant domain-wall-enhanced tunable microwave ferroelectrics, Nature **560**, 622 (2018).
[9] D. Sando, A. Barthélémy, and M. Bibes, $BiFeO_3$ epitaxial thin films and devices: Past, present and future, J. Phys.: Condens. Matter **26**, 473201 (2014).
[10] F. Kubel and H. Schmid, Structure of a ferroelectric and ferroelastic monodomain crystal of the perovskite $BiFeO_3$, Acta Crystallogr. Sect. B: Struct. Sci. **46**, 698 (1990).
[11] I. Sosnowska, T. P. Neumaier, and E. Steichele, Spiral magnetic ordering in bismuth ferrite, J. Phys. C: Solid State Phys. **15**, 4835 (1982).
[12] C. Michel, J.-M. Moreau, G. D. Achenbach, R. Gerson, and W. J. James, The atomic structure of $BiFeO_3$, Solid State Commun. **7**, 701 (1969).
[13] S. K. Streiffer, C. B. Parker, A. E. Romanov, M. J. Lefevre, L. Zhao, J. S. Speck, W. Pompe, C. M. Foster, and G. R. Bai, Domain patterns in epitaxial rhombohedral ferroelectric films, I. Geometry and experiments, J. Appl. Phys. **83**, 2742 (1998).
[14] F. Zavaliche, S. Y. Yang, T. Zhao, Y. H. Chu, M. P. Cruz, C. B. Eom, and R. Ramesh, Multiferroic $BiFeO_3$ films: Domain structure and polarization dynamics, Phase Transit **79**, 991 (2006).
[15] Isabell Gross, W. Akhtar, V. Garcia, L. J. Martínez, Saddem Chouaieb, K. Garcia, C. Carrétéro, A. Barthélémy, P. Appel, P. Maletinsky, J.-V. Kim, J. Y. Chauleau, J. Jaouen, M. Viret, M. Bibes, S. Fusil, and V. Jacques, Real-space imaging of non-collinear antiferromagnetic order with a single-spin magnetometer, Nature **549**, 252 (2017).
[16] Izabela Sosnowska, Radosław PrzeniosŁo, Andrzej Palewicz, Dariusz Wardecki, and Andrew Fitch, Monoclinic deformation of crystal lattice of bulk α-$BiFeO_3$: High resolution synchrotron radiation studies, J. Phys. Soc. Jpn **81**, 044604 (2012).
[17] N. Waterfield Price, R. D. Johnson, W. Saenrang, F. Maccherozzi, S. S. Dhesi, A. Bombardi, F. P. Chmiel, C. B. Eom, and P. G. Radaelli, Coherent Magnetoelastic Domains in Multiferroic $BiFeO_3$ Films, Phys. Rev. Lett. **117**, 177601 (2016).
[18] D. Kan and I. Takeuchi, Effect of substrate orientation on lattice relaxation of epitaxial $BiFeO_3$ thin films, J. Appl. Phys. **108**, 014104 (2010).
[19] See the Supplemental Material at http://link.aps.org/supplemental/10.1103/PhysRevApplied.11.024035 which includes Ref. [33], for further information on the sample growth and characterization, extended nonresonant x-ray magnetic-scattering data and analysis, and further characterization of the switched state.
[20] R. D. Johnson, P. Barone, A. Bombardi, R. J. Bean, S. Picozzi, P. G. Radaelli, Y. S. Oh, S. W. Cheong, and L. C. Chapon, X-Ray Imaging and Multiferroic Coupling of Cycloidal Magnetic Domains in Ferroelectric Monodomain $BiFeO_3$, Phys. Rev. Lett. **110**, 217206 (2013).
[21] J. E. Giencke, C. M. Folkman, S. H. Baek, and C. B. Eom, Tailoring the domain structure of epitaxial $BiFeO_3$ thin films, Curr. Opin. Solid State Mater. Sci. **18**, 39 (2014).
[22] C. M. Folkman, S. H. Baek, H. W. Jang, C. B. Eom, C. T. Nelson, X. Q. Pan, Y. L. Li, L. Q. Chen, A. Kumar, V. Gopalan, and S. K. Streiffer, Stripe domain structure in epitaxial (001) $BiFeO_3$ thin films on orthorhombic $TbScO_3$ substrate, Appl. Phys. Lett. **94**, 251911 (2009).
[23] H. W. Jang, D. Ortiz, S.-H. Baek, C. M. Folkman, R. R. Das, P. Shafer, Y. Chen, C. T. Nelson, X. Pan, R. Ramesh, and C. B. Eom, Domain engineering for enhanced ferroelectric properties of epitaxial (001) $BiFeO_3$ thin films, Adv. Mater. **21**, 817 (2009).
[24] D. D. Fong, A. M. Kolpak, J. A. Eastman, S. K. Streiffer, P. H. Fuoss, G. B. Stephenson, C. Thompson, D. M. Kim, K. J. Choi, C. B. Eom, I. Grinberg, and A. M. Rappe, Stabilization of Monodomain Polarization in Ultrathin $PbTiO_3$ Films, Phys. Rev. Lett. **96**, 127601 (2006).
[25] S. H. Baek, C. M. Folkman, J. W. Park, S. Lee, C. W. Bark, T. Tybell, and C. B. Eom, The nature of polarization fatigue in $BiFeO_3$, Adv. Mater. **23**, 1621 (2011).
[26] X. Zou, L. You, W. Chen, H. Ding, Di Wu, T. Wu, L. Chen, and J. Wang, Mechanism of polarization fatigue in $BiFeO_3$, ACS Nano **6**, 8997 (2012).
[27] S. Lee, T. Choi, W. Ratcliff II, R. Erwin, S.W. Cheong, and V. Kiryukhin, Single ferroelectric and chiral magnetic domain of single-crystalline $BiFeO_3$ in an electric field, Phys. Rev. B **78**, 100101 (2008).
[28] S. Bordács, D. G. Farkas, J. S. White, R. Cubitt, L. DeBeer-Schmitt, T. Ito, and I. Kézsmárki, Magnetic Field Control of Cycloidal Domains and Electric Polarization in Multiferroic $BiFeO_3$, Phys. Rev. Lett. **120**, 147203 (2018).
[29] C-Y. Kuo *et al.*, Single-domain multiferroic $BiFeO_3$ films, Nat. Commun. **7**, 12712 (2016).
[30] W. Saenrang *et al.*, Deterministic and robust room-temperature exchange coupling in monodomain multiferroic $BiFeO_3$ heterostructures, Nat. Commun. **8**, 1583 (2017).
[31] A. Brewer, K. H. Cho, W. Saenrang, S. H. Baek, J. C. Frederick, and C. B. Eom, Uniform sputter deposition

of high-quality epitaxial complex oxide thin films, J. Vac. Sci. Technol. A: Vac. Surf. Films **35**, 060607 (2017).

[32] R. R. Das, D. M. Kim, S. H. Baek, C. B. Eom, F. Zavaliche, S. Y. Yang, R. Ramesh, Y. B. Chen, X. Q. Pan, X. Ke, M. S. Rzchowski, and S. K. Streiffer, Synthesis and ferroelectric properties of epitaxial $BiFeO_3$ thin films grown by sputtering, Appl. Phys. Lett. **88**, 242904 (2006).

[33] M. Blume and D. Gibbs, Polarization dependence of magnetic x-ray scattering, Phys. Rev. B **37**, 1779 (1988).

[34] N. Waterfield Price, R. D. Johnson, W. Saenrang, A. Bombardi, F. P. Chmiel, C. B. Eom, and P. G. Radaelli, Electrical Switching of Magnetic Polarity in a Multiferroic $BiFeO_3$ Device at Room Temperature, Phys. Rev. Appl. **8**, 014033 (2017).

[35] Note that we are primarily sensitive to the r_1 domain but, as can be seen from Fig. 1(b), there will be some finite contribution from r_1' scattering to the same point in reciprocal space.

[36] https://dx.doi.org/10.5287/bodleian:XmRQx18qO.